Mechanics of Advanced Composite Structures 10 (2023) 69 – 84

Semnan University

Mechanics of Advanced Composite Structures

journal homepage: http://MACS.journals.semnan.ac.ir

Free Vibration Analysis of 2D Functionally Graded Porous Beams Using Novel Higher-Order Theory

G. C. M. Reddy [a*], N. V. Kumar [b]

[a] *Research Scholar, Department of Mechanical Engineering, School of Technology, GITAM, Hyderabad, 502329, India.*
[b] *Professor, Department of Mechanical Engineering, School of Technology, GITAM, Hyderabad, 502329, India.*

KEYWORDS

Free vibration behavior
n^{th} order shear deformation theory;
Lagrange's equations;
2D FGB.

ABSTRACT

Functionally graded material (FGM) is an in-homogeneous composite, constructed from various phases of material elements, often ceramic and metal. This work aims to examine the behavior of free vibration in porous Functionally Graded Beams (FGBs) in 2 directions (2D) by using nth-order shear deformation theory. With the help of Hamilton's principle and Reddy's beam theory, equilibrium equations for free vibration were derived. Boundary conditions such as Simply Supported – Simply Supported (SS), Clamped – Clamped (CC) and Clamped-Free (CF) were employed. A unique shear shape function was derived and nth-order theory was adapted to take into account the effect of transverse shear deformation to get zero shear stress conditions at the top and bottom surfaces of the beam. Based on power law, FGB properties were changed in length and thickness directions. The displacement functions in axial directions were articulated in algebraic polynomials, including admissible functions which were used to fulfill different boundary conditions. Convergence and verification were performed on computed results with findings of previous studies. It was found that the results obtained using the nth-order theory were in agreement and allows for better vibration analysis in a porous material.

1. Introduction

Materials have played a significant role in the development of society throughout human history. But in the present scenario, conventional engineering materials are deficient in fulfilling the desired properties, demanded in various applications. To overcome the aforesaid deficiency, advancements in the field of materials are needed.

FGMs are such materials that have a good number of advantages over conventional materials. They largely preserve the characteristics of the components that make them up. According to Li et al. [1], the continuous transition of materials minimizes residual strain, and stress concentration, and offers a good strength-to-weight ratio. These features make FGMs attractive to structural engineers and researchers, and they are leading to be used in broad engineering fields, such as Aerospace, Mechanical, Civil, and Nuclear domains.

1.1. FGMs

Asemi et al. [2] "for the transverse vibration of double-piezoelectric-nano plate systems with initial stress under an external electric voltage, a nonlocal continuum plate model was created". To account for the impact of shearing between two piezoelectric nanoplates in addition to the typical behavior of coupling elastic medium, the Pasternak foundation model was used. Aydogdu et al. [3] based on exponential and power law, the elastic modulus of the beam was varied in a thickness direction. Using shear deformation shell theory, the free vibration behavior of a simply supported FGB was determined. Al-Zahrani et al. [4] Finite element method was used for investigating free vibration in axial and thickness directions of bi-directional FGBs. To describe the changes of volume fraction in metal and ceramic based on the Vogit model.

Barati et al. [5] their paper examined "bi-directional Functionally Graded (FG) nanobeams" exposed to a longitudinal magnetic field in terms

* Corresponding author. Tel.: +91-8297909752
E-mail address: cmreddy115@gmail.com

DOI: 10.22075/macs.2022.28118.1428
Received 2022-08-16; Received in revised form 2022-10-08; Accepted 2022-10-17.

of transverse vibrations. The small-scale effect was taken into account using the nonlocal elasticity hypothesis. Bellifa et al. [6] For bending and dynamic behavior of FG plates, a first-order theory incorporating shear deformation was developed. The governing equations of axial and transverse deformations of functionally graded plates (FGPs) were developed using 1st-order plate theory with shear deformation. Daneshmehr et al. [7], their study examined the small-scale effects on free vibration behavior. The small-scale effects on natural frequencies were investigated using Eringen's nonlocal hypothesis. While stocky and short nanoplates were taken into account, higher-order shear deformation plate theory was adapted to provide more precise results when analyzing the nanoplate. Ebrahimi et al. [8] based on 3rd-order beam theory with shear deformation, free vibration characteristics of FG nanobeams were investigated by presenting a Navier-type solution. Along the thickness direction, the material properties of FG nanobeam were changed continuously as per power law. Hadji et al. [9] "in their study, attention was given to examining nano beam's dynamic stability in a generic condition of non-uniform bending stress. Higher-order deformation theory was used to develop governing equations of motion for FGPs. Zaoui et al. [10] using "an improved hyperbolic shear deformation theory, developed analytical solutions to free vibration analysis of FGBs that included stretching effect".

Haghshenas Gorgani et al. [11], various higher-order shear deformation theories have been established for bending and free vibration of FGPs. The pull-in behavior of FGM cantilever micro/nano-beams under the influence of electrostatic force was studied. By adopting a skew-symmetric portion of rotation gradients, the coupling tensor becomes skew-symmetric fulfilling consistent couple stress theory. Hebbar et al. [12] 2D and quasi-3D theories of shear deformation were used to analyze the behavior of free vibration, static bending, and elastic buckling of FGBs with simply supported. Huang et al. [13] studied composite nanoplate's nonlinear vibration analysis, lipid face sheets and an FG core were used to create a composite nanoplate. The FG core material characteristics vary in three different directions. The viscoelastic impact of lipid layers was investigated using the Kelvin-Voigt model. The "nonlinear differential equation of vibration analysis of composite" nanoplate was obtained" utilizing Von-Karman hypotheses. Jha et al. [14] using "higher-order theory of shear and normal deformation, free vibration analysis of FG elastic, rectangular, and simply supported plates as described". Although heterogeneous, mechanical characteristics of FGM were modified smoothly concerning spatial coordinates. Armagan Karamanli [15], two-directional FGBs behavior of free vibration was presented with various boundary conditions. The properties of beam material were changed by accommodating various gradation exponents in x and z directions. Ketabdari et al. [16], "based on Winkler and Pasternak elastic foundation, the free vibration of homogeneous and FGPs" were tested. The elastic foundation was a combination of Pasternak and Winkler electric support with parabolically and linearly variable stiffness coefficients along the directions. Larbi et al. [17] presented a bending analysis of the free vibration of FGB on the natural surface position of shear deformation theory. Boundary settings were satisfied with no shear correction factor. Mohammadi et al. [18], the "free vibration behavior of a rectangular graphene sheet subjected to a shear in-plane force investigated. "The vibration analysis of "orthotropic single-layered graphene sheets exposed to shear in-plane" force has been studied using nonlocal elasticity theory." Ohab-Yazdi et al. [19], based on the generalized differential quadrature method and minimum total potential energy, derived boundary conditions, and governing equations. In their investigation vibration analysis of 2D, FG nanobeams were done by employing the Euler-Bernoulli theory. Nguyen et al. [20], 1st order beam theory with shear deformation was developed to determine the static and vibration of FGBs. Transverse shear stiffness was improved by using plane stress and equilibrium equation.

Rahmani et al. [21] discussed the effect of size dependency in FGM based on the beam theory of Timoshenko. Along with the thickness, the material properties of FG nanobeams varied based on the power law. Safarabadi et al. [22] considered the surface effect in an investigation of vibration frequencies of nanobeams and for the satisfaction of surface balance equations of continuum surface elasticity, to propose the Gurtin-Murdoch model. Şimşek [23], the fundamental frequency of FGB was investigated using classical, first-order, and third-order theories with various boundary settings. Babaei et al. [24], this study developed a computational 3D finite element approach to examine the static responses and natural frequencies of a saturated FG porous annular elliptical sector plate. Utilizing the Rayleigh-Ritz energy model, the finite element method was used to construct the governing equations. Talha et al. [25], FGM plates were analyzed to determine the behavior of vibration and static, based on a theory of HSD with modification of transverse displacement by finite element model. Thai et al. [26], FGBs were analyzed to determine static bending and vibration analysis with various theories of HSD. With transverse shear strain, boundary settings

satisfy the top and bottom surfaces of the beam. Vo, et al. [27], "an improved theory of shear deformation was developed for the analysis of static bending and vibration of FGBs. The shear correction factor was not necessary by shear deformation theory". Şimşek [28], "Free and forced vibration of a Timoshenko beam with bi-directional FGM was explored under the influence of a moving load". In both axial and thickness dimensions, the beam characteristics varied exponentially. Sayyad et al. [29], the theory of unified shear deformation was developed based on displacement for analysis of advanced composite plates and beams. This theory considered shape function in terms of the transverse shear deformation effect. Razouki et al. [30], under UDL, developed exact analytical results of a simply supported beam. Specific analytical formulas were expressed by using 3rd-order shear deformation and compared to existing numerical results and classical analytical ones.

1.2. Porous FGMs

Slimane et al. [31], using higher order shear deformation theory, free vibration analysis of a simply supported FGP with porosity was investigated. The material characteristics of FG porous plate changed over a thickness of plate. Mehdianfar et al. [32], investigated on analysis of free vibration of 2D porous FG sandwich beams by using the Galerkin method. From Hamilton's principle, the motion equations of the beam were derived. This theory didn't require a shear correction factor. In this, the analytical values were compared with Timoshenko's first-order parabolic shear deformation theory. Asemi et al. [33], this research investigated for the first time static, dynamic, and natural frequency assessments of FG porous annular sector plate reinforced by graphene nanoplatelets. The plate was made up of a layered model with a metallic matrix that has open-cell interior pores and graphene platelets that are dispersed uniformly or unevenly. Babaei et al. [34], this research investigated natural frequencies and dynamic responses of thick beams formed of saturated porous materials resting on a viscoelastic foundation. Higher-order beam theory was utilized to model the beam. The viscoelastic basis was modeled using the Kelvin-Voight equation. Mohammadi et al. [35], Lipid face sheets and an FG core were used to create a composite nanoplate to study the composite nanoplate's nonlinear vibration analysis. The FG core's material characteristics vary in three different directions. The viscoelastic impact of lipid layers was investigated using the Kelvin-Voigt model. Nonlinear differential equation of vibration analysis for composite nanoplate was obtained utilizing Von-Karman hypotheses.

Kim et al. [36] by using classical and first-order shear deformation plate theories, the bending, free vibration, and buckling responses of FG porous micro-plates were investigated. Chen et al. [37] presented free vibration analysis of linear and nonlinear rotating FG porous beams by employing Timoshenko beam theory, modified couple of stresses, and assumptions of Von Karman Geometric nonlinearity. Li et al. [38] investigated buckling, free vibration, and bending analysis of 2D FGPs by using isogeometric analysis and first-order shear deformation theory. The governing equations of porous 2D FG plates were derived by employing Hamilton's principle. Bathini et al. [39] investigated the free vibration behavior of bi-directional FGPs from a refined theory of shear deformation with first order. From Lagrange equations, equations of motion were obtained. Kumar et al. [40], based on classical plate theory to investigated transverse vibration in thin isotropic simply supported FG rectangular plates with the effect of porosity. The plate is positioned elastically against rotation. Vasara et al. [41], investigated non-axisymmetric free vibration in 2D FGPs with porosity by using first-order theory. By employing gradient index in both directions and porosity distribution in different ways.

The fabrication of FGMs can be done in a variety of ways, including vapor deposition, self-propagating high-temperature synthesis, powder metallurgy, non-pressure sintering, and multistep sequential infiltration. Porosities and micro-voids, however, may appear in the material created during the sintering process when FGMs are produced. This is a result of the ceramic phase being at a comparatively low temperature while the metal phase coagulated at a very high temperature. The strength of the material will be exotically weakened by the pores. When constructing bidirectional FGM components, it is essential to evaluate the porosity effect.

From the literature, it is observed that most studies dealt with analysis on non-porous FGM such as beams, and plates using first and second order theories in one direction". This intrigued us to investigate the effect of porosity in two directions in FGM adapting n^{th} order theory.

"The objective of this paper is to focus on the free vibration behavior of 2D-FGBs with porosity based on a power-law variation of material properties with various end conditions, aspect ratios, gradient indexes, and porosity index". A unique shear shape function was derived and n^{th} order theory was adapted to take into account the effect of transverse shear deformation to get zero shear stress conditions at the top and bottom surfaces of FGB.

2. Materials and Methods

In this research work, a rectangular beam of FGM with length L in the x-direction, width b in the y-direction, and thickness h in the z-direction is considered as shown in Fig. 1. Variation of beam material along the length direction, in this situation the material gradient is changed from left (-L/2) to right (L/2) and in the thickness direction, FGM rectangular beam is created by grading ceramic and metal phases. Here, the upper surface (z= +h/2) with metal and the lower surface (z=-h/2) with ceramic. The middle surface of the beam is the reference surface i.e. (z=0).

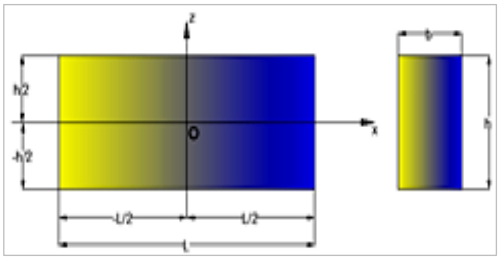

Fig. 1. Geometry of Functionally Graded Beam

Material properties of FGBs are the function of the volume fraction of constituent materials. The functional relationship between thickness coordinates and material properties is assumed. The volume fraction of material according to power-law distribution in two directions (x and z) is expressed in Eq. 1[42].

$$V_f(x,z) = \left(\frac{z}{h}+\frac{1}{2}\right)^{p_z}\left(\frac{x}{L}+\frac{1}{2}\right)^{p_x} \quad (1)$$

where, h and z represent the thickness of the beam and thickness coordinate, and L and x represent the length of the beam and length coordinate respectively. Origin (O) is the rectangular beam's mid surface (x, y) thus z ϵ [-h/2, h/2]. 'p' indicates the volume fraction behavior along the beam's thickness and length. Figure 2 shows a variation of volume fractions of metal in thickness and length direction.

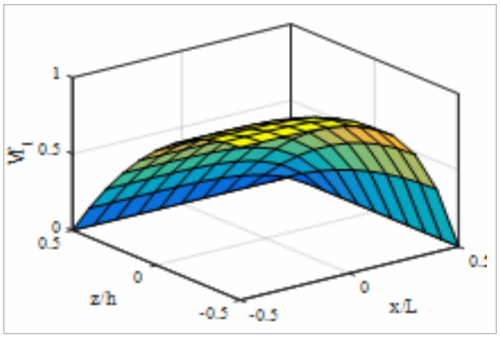

Fig. 2. Volume fractions of metal in thickness (z/h) and length (x/L) direction.

2.1. Formulation for Functionally Graded Porous Beams

Porosities appear as a defect in FGBs because of technical and penetration problems in the production process. Porosities in the beam are two types namely even and uneven as shown in Fig. 3. The properties of efficient material of FG beams such as Modulus of elasticity E, Poisson's ratio μ and mass density ρ, are to be found by using a modified rule of the mixture in which the porosity is represented by α, which affects averagely on the material volume fraction of each constituent. As a result, the material property P(x, z) can be written for each type of porosity in coordinates of the x and z directions.

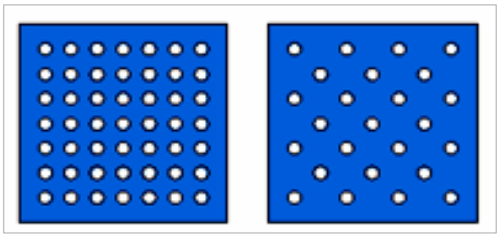

Fig. 3. Representation of bi-directional FGB with even and uneven porosity distributions

Material properties of the FGM porous beam (even distribution) are presented in Eq.2 [43].

$$P(x,z) = (P_c - P_m)\left(\frac{z}{h}+\frac{1}{2}\right)^{p_z}\left(\frac{x}{L}+\frac{1}{2}\right)^{p_x} + P_m - \frac{\alpha}{2}(P_c + P_m) \quad (2)$$

here α represents the coefficient of porosity which can be defined as the ratio between void volume and complete volume (0 ≤ α< 1). The subscripts m denotes the metal and c denote ceramic phases. 'P_x' and 'P_z' is non-negative variables that define AFG (along an axis) and FG (along thickness) power indexes, respectively. These are related to volume fraction change along axis and thickness. The material properties of the beam, i.e. Young's Modulus 'E' and mass density 'ρ' of FGM porous beam (even) are given in Eq. 3, Eq. 4.

$$E(x,z) = (E_c - E_m)\left(\frac{z}{h}+\frac{1}{2}\right)^{p_z}\left(\frac{x}{L}+\frac{1}{2}\right)^{p_x} + E_m - \frac{\alpha}{2}(E_c + E_m) \quad (3)$$

$$\rho(x,z) = (\rho_c - \rho_m)\left(\frac{z}{h}+\frac{1}{2}\right)^{p_z}\left(\frac{x}{L}+\frac{1}{2}\right)^{p_x} + \rho_m - \frac{\alpha}{2}(\rho_c + \rho_m) \quad (4)$$

The material properties of the beam, i.e. Young's Modulus 'E' and mass density 'ρ' of FGM porous beam (uneven) are given below in Eq. 5, Eq. 6.

$$(x,z) = (E_c - E_m)\left(\frac{z}{h}+\frac{1}{2}\right)^{p_z}\left(\frac{x}{L}+\frac{1}{2}\right)^{p_x} + E_m - \frac{\alpha}{2}(E_c + E_m)\left(1 - \frac{2|z}{h}\right) \quad (5)$$

$$\rho(x,z) = (\rho_c - \rho_m)\left(\frac{z}{h}+\frac{1}{2}\right)^{p_z}\left(\frac{x}{L}+\frac{1}{2}\right)^{p_x} + \rho_m - \frac{\alpha}{2}(\rho_c + \rho_m)\left(1 - \frac{2|z}{h}\right) \quad (6)$$

2.2. Displacement Field and Constitutive Equations

Consider the FG rectangular beam as shown in Fig.1. for an analytical result of vibration analysis. The accurate vibration of beams depends upon transverse shear and normal deformation. Therefore any refinement of classical beam theory is generally meaningless. In this regard, the effect of transverse shear and normal strain is considered. The present theory has important features as follows:

The displacement equations are based on Reddy's advanced refined higher-order beam theory.

$$U(x,z,t) = u_0(x,t) + z\emptyset(x,t) - f\left(\emptyset(x,t) + \frac{\partial w_0}{\partial x}(x,t)\right) \quad (7)$$

$$W(x,z,t) = w_0(x,t) \quad (8)$$

From the above equations, u is axial displacement, w is transverse displacement, and u_0, w_0 is the axial displacement at any point on the neutral axis, $\frac{\partial w_0}{\partial x}$ is the bending slope and ϕ is a shear slope. For determining the distribution of transverse shear deformation shape function $i.e.f(z)$.

$$\varepsilon_x = \frac{\partial U}{\partial x} = \frac{\partial u_0}{\partial x} - z\frac{\partial^2 w_0}{\partial x^2} + f\left(\frac{\partial \phi}{\partial x} + \frac{\partial^2 w_0}{\partial x^2}\right) \quad (9)$$

$$\varepsilon_z = \frac{\partial w}{\partial z} = 0 \quad (10)$$

$$\gamma_{xz} = f'\left[\emptyset + \frac{\partial w_0}{\partial x}\right] \quad (11)$$

$$f = \frac{h}{\pi} * sin\left[\frac{\pi * z}{h}\right] - \frac{z}{n*\pi}\left(1 - \frac{1}{n} * \left(\frac{2}{h}\right)^{n-1} * z^{n-1}\right) \quad (12)$$

$$f' = \frac{h}{\pi} * sin\left[\frac{\pi}{h}\right] - \frac{1}{n*\pi}\left(1 - \frac{1}{n} * \left(\frac{2}{h}\right)^{n-1} * (n-1)z^{n-2}\right) \quad (13)$$

The relationship between stress and strain of two directional FGM beam coordinate axes is given by,

$$\sigma_x = \frac{E(x,z)}{1-\mu^2}\varepsilon_x \quad (14)$$

$$\tau_{xz} = \frac{E(x,z)}{2(1+\mu)}\gamma_{xz} \quad (15)$$

2.3. Governing Equations of Motion

From the principle of Hamilton, the equations of motion are derived and can be stated in time intervals [0,t] as,

$$\int_0^T \delta(U - K)\, dt = 0 \quad (16)$$

where δU is the variation of strain energy, and δk is the variation of kinetic energy respectively.

2.4. Formulation of Free Vibration

The strain energy of bi-directional FGB can be written as:

$$U = \frac{1}{2}\int_0^L \int_{-\frac{h}{2}}^{+\frac{h}{2}} (\sigma_x\varepsilon_x + \tau_{xz}\gamma_{xz})dzdx \quad (17)$$

Substituting Eq. (9), Eq. (11), Eq. (14), and Eq.(15) into Eq. (17) the strain energy can be written as,

$$\mathrm{U} = \frac{1}{2}\int_0^{\mathrm{L}} \int_{-\frac{\mathrm{h}}{2}}^{+\frac{\mathrm{h}}{2}} \left[\left(\frac{\mathrm{E(x,z)}}{1-\mu^2}\left(\left(\frac{\partial \mathrm{u_0}}{\partial \mathrm{x}}\right)^2 - 2\mathrm{f}\frac{\partial \mathrm{u_0}}{\partial \mathrm{x}}\frac{\mathrm{d}^2\mathrm{w_0}}{\mathrm{dx}^2} + (2\mathrm{z} - 2\mathrm{f})\frac{\partial \mathrm{u_0}}{\partial \mathrm{x}}\frac{\partial \phi}{\partial \mathrm{x}} + \mathrm{f}^2\left(\frac{\mathrm{d}^2\mathrm{w_0}}{\mathrm{dx}^2}\right)^2 + \frac{\mathrm{d}^2\mathrm{w_0}}{\mathrm{dx}^2}\frac{\partial \phi}{\partial \mathrm{x}}(2\mathrm{f}^2 - 2\mathrm{zf}) + \left(\frac{\partial \phi}{\partial \mathrm{x}}\right)^2(\mathrm{z}^2 - 2\mathrm{zf} + \mathrm{f}^2)\right)\right) + \frac{\mathrm{E(x,z)}}{2(1+\mu)}\left(\phi^2(1 - 2\mathrm{f}' + (\mathrm{f}')^2 + \phi\frac{\partial \mathrm{w_0}}{\partial \mathrm{x}}(2 - 4\mathrm{f}'^{-}2\mathrm{f}'^{2}) + \left(\frac{\mathrm{dw_0}}{\mathrm{dx}}\right)^2(1 - 2\mathrm{f}' - (\mathrm{f}')^2)\right)\right]\mathrm{dzdx} \quad (18)$$

$$(A,B,C,D,F,H) = \int_{-\frac{\mathrm{h}}{2}}^{+\frac{\mathrm{h}}{2}} (1, \mathrm{z}, \mathrm{f}', \mathrm{f}, (\mathrm{f}')^2, (\mathrm{f})^2)\mathrm{dz} \quad (18a)$$

$$\mathrm{U} = \frac{1}{2}\int_0^{\mathrm{L}} \int_{-\frac{\mathrm{h}}{2}}^{+\frac{\mathrm{h}}{2}} \left[\left(\frac{\mathrm{E(x,z)}}{1-\mu^2}\left(\mathrm{A}\left(\frac{\partial \mathrm{u_0}}{\partial \mathrm{x}}\right)^2 - 2\mathrm{D}\frac{\partial \mathrm{u_0}}{\partial \mathrm{x}}\frac{\mathrm{d}^2\mathrm{w_0}}{\mathrm{dx}^2} + (2\mathrm{B} - 2\mathrm{D})\frac{\partial \mathrm{u_0}}{\partial \mathrm{x}}\frac{\partial \phi}{\partial \mathrm{x}} + \mathrm{H}\left(\frac{\mathrm{d}^2\mathrm{w_0}}{\mathrm{dx}^2}\right)^2 + \frac{\mathrm{d}^2\mathrm{w_0}}{\mathrm{dx}^2}\frac{\partial \phi}{\partial \mathrm{x}}(2\mathrm{H} - 2\mathrm{BD}) + \left(\frac{\partial \phi}{\partial \mathrm{x}}\right)^2(\mathrm{C} - 2\mathrm{BD} + \mathrm{H})\right)\right) + \frac{\mathrm{E(x,z)}}{2(1+\mu)}\left(\phi^2(1 - 2\mathrm{C} + \mathrm{H}) + \phi\frac{\partial \mathrm{w_0}}{\partial \mathrm{x}}(2 - 4\mathrm{C} - 2\mathrm{F}) + \left(\frac{\mathrm{dw_0}}{\mathrm{dx}}\right)^2(1 - 2\mathrm{C} - \mathrm{F})\right)\right]\mathrm{dx} \quad (18b)$$

The kinetic energy of bi-directional FGB can be written similarly:

$$(\mathrm{I_0}, \mathrm{I_1}, \mathrm{I_2}, \mathrm{J_1}, \mathrm{J_2}, \mathrm{K_1}) = \int_{-\frac{\mathrm{h}}{2}}^{+\frac{\mathrm{h}}{2}} (1, \mathrm{z}, \mathrm{f}', \mathrm{f}, (\mathrm{f}')^2, (\mathrm{f})^2) \tag{18c}$$

$$K = \frac{1}{2}\int_0^L \int_{-\frac{h}{2}}^{+\frac{h}{2}} \left[\left(\rho(\mathrm{x}, z) \frac{\mathrm{E(x,z)}}{1-\mu^2} \left(I_0 \left(\frac{\partial u_0}{\partial t} \right)^2 - 2J_1 \frac{\partial u_0}{\partial t} \frac{d^2 w_0}{dxdt} + (2I_1 - 2J_1) \frac{\partial u_0}{\partial t} \frac{\partial \phi}{\partial t} + K_1 \left(\frac{d^2 w_0}{\partial xdt} \right)^2 + (2I_1 - 2I_1 J_1) \frac{d^2 w_0}{dxdt} \frac{\partial \phi}{\partial t} + (I_2 - 2I_1 J_1 + K_1) \left(\frac{\partial \phi}{\partial t} \right)^2 \right) \right) + \rho(\mathrm{x}, z) \frac{E(\mathrm{x,z})}{2(1+\mu)} \left(\phi^2 (1 - 2I_2 + K_1) + \phi \frac{\partial w_0}{\partial t} (2 - 4I_2 - 2J_2) + \left(\frac{d^2 w_0}{dxdt} \right)^2 (1 - 2I_2 - J_2) \right) \right] dx \tag{19}$$

The kinematic boundary conditions expressed in Lagrange equations from Hamilton's principle are expressed in infinity dimensions in terms of generalized coordinators and are presented in displacement functions as,

$$u_0(x,t) = \sum_{j=1}^{m} A_j \theta_j(x) e^{i\omega t}, \quad \theta_j(x) = \left(x + \frac{L}{2} \right)^{p_u} \left(x - \frac{L}{2} \right)^{q_u} x^{m-1} \tag{20}$$

$$w_0(x,t) = \sum_{j=1}^{m} B_j \varphi_j(x) e^{i\omega t}, \quad \varphi_j(x) = \left(x + \frac{L}{2} \right)^{p_w} \left(x - \frac{L}{2} \right)^{q_w} x^{m-1} \tag{21}$$

$$\phi(x,t) = \sum_{j=1}^{m} C_j \psi_j(x) e^{i\omega t}, \quad \psi_j(x) = \left(x + \frac{L}{2} \right)^{p_\phi} \left(x - \frac{L}{2} \right)^{q_\phi} x^{m-1} \tag{22}$$

Proposed $\theta_j(x)$, $\varphi_j(x)$, and $\psi_j(x)$ are shape functions in the natural frequency of beam, and $i = \sqrt{-1}$ complex numbers are used in determining unknown coefficients A_j, B_j, and C_j.

By substituting equations 20, 21, and 22 into 18 & 19 and got governing equations of motion.

$$\frac{\partial \mathrm{U}}{\partial \mathrm{q_j}} + \frac{\partial}{\mathrm{dt}} \left(\frac{\partial \mathrm{k}}{\partial \mathrm{q_j}} \right) = 0 \tag{23}$$

The values of A_j, B_j, and C_j represented with q_j, lead to:

$$\begin{bmatrix} [S_{11}] & [S_{12}] & [S_{13}] \\ [S_{12}]^T & [S_{22}] & [S_{23}] \\ [S_{13}]^T & [S_{23}]^T & [S_{33}] \end{bmatrix} - \omega^2 \begin{bmatrix} [M_{11}] & [M_{12}] & [M_{13}] \\ [M_{12}]^T & [M_{22}] & [M_{23}] \\ [M_{13}]^T & [M_{23}]^T & [M_{33}] \end{bmatrix} \begin{Bmatrix} A \\ B \\ C \end{Bmatrix} = \begin{Bmatrix} \{0\} \\ \{0\} \\ \{0\} \end{Bmatrix} \tag{24}$$

The stiffness and mass matrices are [Ski] and [Mki], respectively. The stiffness and mass matrices should be symmetric and in max size. The stiffness and mass matrix components are given by,

$$S_{11}(i,j) = \mathrm{A} \int_{-L/2}^{L/2} \frac{E(x,z)}{1-\mu^2} \theta_{i,x} \theta_{j,x} dx \tag{25}$$

$$S_{12}(i,j) = -D \int_{-L/2}^{L/2} \frac{E(x,z)}{1-\mu^2} \theta_{i,x} \varphi_{j,xx} dx \tag{26}$$

$$S_{13}(i,j) = (B - D) \int_{-L/2}^{L/2} \frac{E(x,z)}{1-\mu^2} \theta_{i,x} \psi_{j,x} dx \tag{27}$$

$$S_{22}(i,j) = \mathrm{H} \int_{-\frac{L}{2}}^{\frac{L}{2}} \frac{E(x,z)}{1-\mu^2} \varphi_{i,xx} \varphi_{j,xx}\, dx + (1 - 2\mathrm{C} - \mathrm{F}) \int_{-\frac{L}{2}}^{\frac{L}{2}} \frac{E(x,z)}{2(1+\mu)} \varphi_{i,x} \varphi_{j,x} dx \tag{28}$$

$$S_{23}(i,j) = (2\mathrm{H} - 2\mathrm{BD}) \int_{-\frac{L}{2}}^{\frac{L}{2}} \frac{E(x,z)}{1-\mu^2} \varphi_{i,xx} \psi_{j,x} dx + (2 - 4I_2 - 2J_2) \int_{-\frac{L}{2}}^{\frac{L}{2}} \frac{E(x,z)}{2(1+\mu)} \varphi_{i,x} \psi_j dx \tag{29}$$

$$S_{33}(i,j) = \mathrm{C} - 2\mathrm{BD} + \mathrm{H} \int_{-\frac{L}{2}}^{\frac{L}{2}} \frac{E(x,z)}{1-\mu^2} \psi_{i,x} \psi_{j,x} dx + (1 - 2\mathrm{C} + \mathrm{H}) \int_{-\frac{L}{2}}^{\frac{L}{2}} \frac{E(x,z)}{2(1+\mu)} \psi_i \psi_j dx \tag{30}$$

$$M_{11}(i,j) = I_0 \int_{-L/2}^{L/2} \rho(x,z) \frac{\mathrm{E(x,z)}}{1-\mu^2} \theta_i \theta_j dx \tag{31}$$

$$M_{12}(i,j) = -2J_1 \int_{-L/2}^{L/2} \rho(z) \frac{\mathrm{E(x,z)}}{1-\mu^2} \theta_i \varphi_{j,x} dx \tag{32}$$

$$M_{13}(i,j) = 2I_1 - 2J_1 \int_{-L/2}^{L/2} \rho(x,z) \frac{\mathrm{E(x,z)}}{1-\mu^2} \theta_i \psi_j dx \tag{33}$$

$$M_{22}(i,j) = K_1 \int_{-\frac{L}{2}}^{\frac{L}{2}} \rho(x,z) \frac{\mathrm{E(x,z)}}{1-\mu^2} \varphi_i \varphi_j dx + (1 - 2I_2 - J_2) \int_{-\frac{L}{2}}^{\frac{L}{2}} \rho(x,z) \frac{E(\mathrm{x,z})}{2(1+\mu)} \varphi_{i,x} \varphi_{j,x} dx \tag{34}$$

$$M_{23}(i,j) = 2I_1 - 2I_1 J_1 \int_{-\frac{L}{2}}^{\frac{L}{2}} \rho(x,z) \frac{\mathrm{E(x,z)}}{1-\mu^2} \varphi_{i,x} \psi_j dx \tag{35}$$

$$M_{33}(i,j) = (I_2 - 2I_1 J_1 + K_1) \times \int_{-\frac{L}{2}}^{\frac{L}{2}} \rho(x,z) \frac{E(x,z)}{1-\mu^2} \psi_i \psi_j dx \tag{36}$$

3. Results and Discussion

Free vibration analysis of 2D FGBs, "which are affected by thickness ratio, aspect ratio, gradation indexes, type of porosity, and volume fraction porosity, is presented. The numerical investigations on Simply Supported (SS), Clamped-Clamped (CC), and Clamped-Free (CF) beam at different boundary conditions are carried out" as shown in Table 1.

Table 1. Various kinematic boundary conditions for numerical computations.

Boundary condition	X= -L/2	X= L/2
Simply Supported	u=0, w=0	w=0
Clamped-Camped	u=0, w=0, ϕ=0, w'=0	u=0,w=0, ϕ=0, w'=0
Clamped-Free	u=0, w=0, ϕ=0, w'=0	

Free vibration behavior is presented to discuss and validate the accuracy of the current theory. FGM porous beam is considered for numerical results, made of Alumina and Aluminum with material properties as follows:

Alumina: E_c=380 GPa $\rho_c = 3960$ kg/m^3 $\mu_c = 0.3$

Aluminum: E_m=70 GPa $\rho_m = 2702$ kg/m^3 μ_m=0.3

According to power-law distribution, the FGB material properties are varying in thickness (h) and axial (L) directions. For a representation of results, the following dimensionless natural frequency (λ) parameter is used:

$$\lambda = \frac{\omega L^2}{h}\sqrt{\frac{\rho_m}{E_m}} \tag{37}$$

Consider the homogeneous beam and a different number of terms with displacement functions. The result of dimensionless free vibration is presented with various gradient indexes in x and z directions, aspect ratios, and boundary conditions. For comparison purpose, previous result [15, 28] was used in terms of free vibration as shown in Table 2, Table 3, Table 4, Table 5, Table 6, and Table 7. It can be observed that in dimensionless free vibration of SS, CC, and CF beams, the response was very quick and polynomial expansion is at 6 in the SS beam and 4 in CC and CF beams. But for better accuracy purposes, polynomial expansion at 12 terms was considered. In terms of aspect ratios (L/h=5 and L/h=20) and gradient indexes in both directions, dimensionless free vibration decreases in SS, CC, and CF beams as the gradient indexes increases in both directions. On the other hand, the dimensionless natural frequency of the CC beam increases in the x-direction and decreases in the z-direction as the gradient index value increase, this is due to the end conditions and reactions.

From the result, the elasticity modulus and stiffness of the beam increase subsequently with an increase in gradient indexes. The frequencies have raised as since the gradient indexes and elasticity modulus increase along with the stiffness of the beam. Of course, this is accurate provided that the beam's mass remains constant. Anyhow in the study mass is not consistent and it is increased by gradient indexes of material. According to vibration theory, the vibration frequency is inversely proportional to mass and directly proportional to the rigidity (also known as elasticity modulus). Then it can be inferred that the effect of modulus of elasticity is more on dimensionless fundamental frequency and the effect of mass is less on the dimensionless fundamental frequency. But the valves of elasticity modulus and mass can compensate for the dimensionless fundamental frequency. However, it is observed that the effect of mass is slightly more than the effect of elasticity modules on frequency. Another important observation is that the effect of gradient indexes (p_x, p_z) is different on frequencies. This effect is dependent upon the boundary conditions. From observation, the effect of gradient indexes on the frequency of SS and CC beam is the same, but the gradient index in the x-direction is more effective than the gradient index in the z-direction as shown in Table 4 and Table 5. In the CF beam, the effect of the gradient index in the z-direction is more than in the x-direction of the gradient index on frequency. Finally, the frequency is more in the CC beam and followed by SS and CF beams as shown in Table 2, Table 3, Table 4, Table 5, Table 6, and Table 7. It is found that the aspect ratio effect becomes very important because, the free vibration increases as the aspect ratio increases, refer to Fig. 4. Fig.5, and Fig. 6.

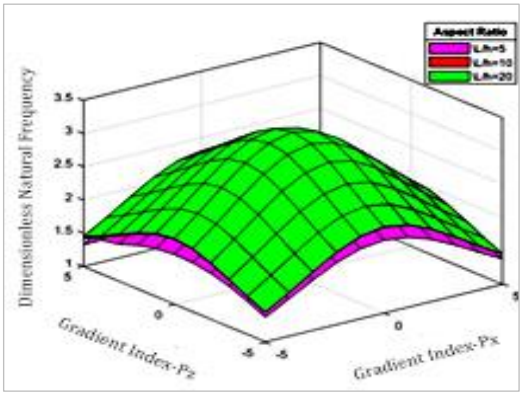

Fig. 4. Changes in dimensionless natural frequencies of SS beam at various aspect ratios along the x-direction gradient index and z-direction gradient index.

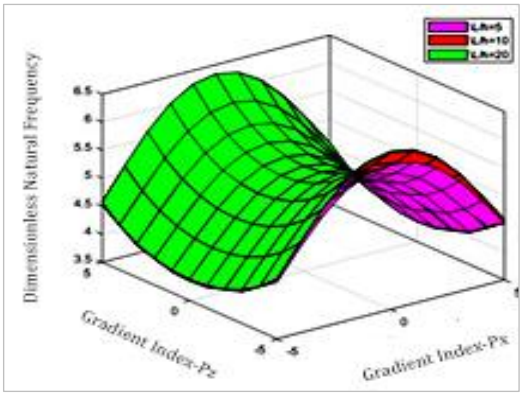

Fig. 5. Changes in dimensionless natural frequencies of CC beam at various aspect ratios along the x-direction gradient index and z-direction gradient index.

Table 2. Influence of gradient indexes and aspect ratio on dimensionless natural frequencies of SS bi-directional FGB, L/h=5

Beam Theory		Px	L/h=5 Pz					
			0	0.2	0.4	0.6	0.8	1
Timoshenko [30]			2.6767	2.6748	2.6669	2.6533	2.6337	2.6103
RBT [17]			2.6773	2.6746	2.6665	2.6532	2.6347	2.6114
PRESENT	2 terms	0	2.9619	2.9589	2.9501	2.9428	2.9224	2.8968
	4 terms		2.6782	2.6756	2.6672	2.6546	2.6371	2.6136
	6 terms		2.6774	2.6748	2.6664	2.6538	2.6346	2.6118
	8 terms		2.6774	2.6748	2.6664	2.6538	2.6346	2.6118
	10 terms		2.6774	2.6748	2.6664	2.6538	2.6346	2.6118
	12 terms		2.6774	2.6748	2.6664	2.6538	2.6346	2.6118
Timoshenko [30]			2.6728	2.6689	2.6611	2.6474	2.6279	2.6044
RBT [17]			2.6722	2.6694	2.6613	2.6479	2.6293	2.6059
PRESENT	2 terms	0.4	2.9614	2.9583	2.9490	2.9338	2.9128	2.8864
	4 terms		2.6733	2.6707	2.6629	2.6501	2.6323	2.6099
	6 terms		2.6725	2.6699	2.6615	2.6478	2.6289	2.6061
	8terms		2.6725	2.6699	2.6615	2.6478	2.6289	2.6061
	10terms		2.6725	2.6699	2.6615	2.6478	2.6289	2.6061
	12terms		2.6725	2.6699	2.6615	2.6478	2.6289	2.6061
Timoshenko [30]			2.6455	2.6416	2.6337	2.6201	2.6005	2.5771
RBT [17]			2.6452	2.6425	2.6418	2.6208	2.6022	2.5788
PRESENT	2 terms	1	2.9145	2.9112	2.9015	2.8854	2.8626	2.8351
	4 terms		2.6463	2.6436	2.6357	2.6225	2.6036	2.5808
	6 terms		2.6451	2.6416	2.6337	2.6205	2.6025	2.5792
	8terms		2.6451	2.6416	2.6337	2.6205	2.6025	2.5792
	10terms		2.6451	2.6416	2.6337	2.6205	2.6025	2.5792
	12terms		2.6451	2.6416	2.6337	2.6205	2.6025	2.5792

Table 3. Influence of gradient indexes and aspect ratio on dimensionless natural frequencies of SS bi-directional FGB, L/h=20

Beam Theory		Px	L/h=20 Pz					
			0	0.2	0.4	0.6	0.8	1
Timoshenko [30]			2.8369	2.8349	2.8251	2.8115	2.7919	2.7685
RBT [17]			2.8371	2.8343	2.8258	2.8118	2.7925	2.7681
PRESENT	2 terms	0	3.1487	3.1455	3.1361	3.1206	3.0992	3.0721
	4 terms		2.8377	2.8349	2.8265	2.8125	2.7933	2.7689
	6 terms		2.8369	2.8340	2.8256	2.8117	2.7924	2.7681
	8 terms		2.8369	2.8340	2.8256	2.8117	2.7924	2.7681
	10 terms		2.8369	2.8340	2.8256	2.8117	2.7924	2.7681
	12 terms		2.8369	2.8340	2.8256	2.8117	2.7924	2.7681
Timoshenko [30]			2.8330	2.8291	2.8212	2.8076	2.7880	2.7626
RBT [17]			2.8326	2.8298	2.8213	2.8073	2.7880	2.7636
PRESENT	2 terms	0.4	3.1386	3.1355	3.1261	3.1106	3.0892	3.0621
	4 terms		2.8332	2.8303	2.8219	2.8080	2.7887	2.7644
	6 terms		2.8324	2.8296	2.8212	2.8072	2.7880	2.7637
	8terms		2.8324	2.8296	2.8212	2.8072	2.7880	2.7637
	10terms		2.8324	2.8296	2.8212	2.8072	2.7880	2.7637
	12terms		2.8324	2.8296	2.8212	2.8072	2.7880	2.7637
Timoshenko [30]			2.8096	2.8056	2.7978	2.7841	2.7646	2.7412
RBT [17]			2.8089	2.8061	2.7977	2.7839	2.7647	2.7405
PRESENT	2 terms	1	3.0878	3.0847	3.0755	3.0601	3.0390	3.0122
	4 terms		2.8095	2.8067	2.7983	2.7845	2.7654	2.7412
	6 terms		2.8091	2.8063	2.7979	2.7841	2.7650	2.7408
	8terms		2.8091	2.8063	2.7979	2.7841	2.7650	2.7408
	10terms		2.8091	2.8063	2.7979	2.7841	2.7650	2.7408
	12terms		2.8091	2.8063	2.7979	2.7841	2.7650	2.7408

Table 4. Influence of gradient indexes and aspect ratio on dimensionless natural frequencies of CC bi-directional FGB, L/h=5.

Beam Theory		Px	L/h=5 Pz					
			0	0.2	0.4	0.6	0.8	1
Timoshenko [30]			5.1943	5.1904	5.1806	5.1630	5.1396	5.1083
RBT [17]			5.2314	5.2274	5.2155	5.1958	5.1685	5.1339
PRESENT	2 terms	0	5.2515	5.2485	5.2393	5.2241	5.2025	5.1746
	4 terms		5.2328	5.2299	5.2208	5.2056	5.1841	5.1563
	6 terms		5.2328	5.2298	5.2207	5.2055	5.1840	5.1562
	8terms		5.2328	5.2298	5.2207	5.2055	5.1840	5.1562
	10 terms		5.2328	5.2298	5.2207	5.2055	5.1840	5.1562
	12 terms		5.2328	5.2298	5.2207	5.2055	5.1840	5.1562
Timoshenko [30]			5.1982	5.1943	5.1845	5.1669	5.1435	5.1123
RBT [17]			5.2356	5.2316	5.2197	5.2000	5.1727	5.1381
PRESENT	2 terms	0.4	5.2612	5.2582	5.2492	5.2340	5.2127	5.1850
	4 terms		5.2376	5.2347	5.2256	5.2164	5.1889	5.1611
	6 terms		5.2376	5.2346	5.2255	5.2163	5.1888	5.1609
	8terms		5.2376	5.2346	5.2255	5.2163	5.1888	5.1609
	10 terms		5.2376	5.2346	5.2255	5.2163	5.1888	5.1609
	12 terms		5.2376	5.2346	5.2255	5.2163	5.1888	5.1609
Timoshenko [30]			5.2197	5.2177	5.2060	5.1884	5.1650	5.1337
RBT [17]			5.2580	5.2540	5.2421	5.2223	5.1949	5.1601
PRESENT	2 terms	1	5.3123	5.3095	5.3008	5.2864	5.2660	5.2394
	4 terms		5.2631	5.2603	5.2512	5.2359	5.2144	5.1864
	6 terms		5.2631	5.2601	5.2510	5.2357	5.2141	5.1862
	8terms		5.2631	5.2601	5.2510	5.2357	5.2141	5.1862
	10 terms		5.2631	5.2601	5.2510	5.2357	5.2141	5.1862
	12 terms		5.2631	5.2601	5.2510	5.2357	5.2141	5.1862

Table 5. Influence of gradient indexes and aspect ratio on dimensionless natural frequencies of CC bi-directional FGB, L/h=20

Beam Theory		Px	L/h=20 Pz					
			0	0.2	0.4	0.6	0.8	1
Timoshenko [30]			6.3486	6.3427	6.3251	6.2939	6.2529	6.2001
RBT [17]			6.3513	6.3451	6.3266	6.2690	6.2537	6.2002
PRESENT	2 terms	0	6.3734	6.3673	6.3491	6.3189	6.2772	6.2244
	4 terms		6.3514	6.3455	6.3273	6.2973	6.2557	6.2031
	6 terms		6.3514	6.3453	6.3272	6.2972	6.2556	6.2029
	8terms		6.3514	6.3453	6.3272	6.2972	6.2556	6.2029
	10 terms		6.3514	6.3453	6.3272	6.2972	6.2556	6.2029
	12 terms		6.3514	6.3453	6.3272	6.2972	6.2556	6.2029
Timoshenko [30]			6.3564	6.3486	6.3310	6.2998	6.2587	6.2060
RBT [17]			6.3575	6.3513	6.3327	6.3021	6.2597	6.2062
PRESENT	2 terms	0.4	6.3785	6.3725	6.3545	6.3247	6.2835	6.2312
	4 terms		6.3578	6.3517	6.3335	6.3035	6.2618	6.2091
	6 terms		6.3577	6.3516	6.3334	6.3033	6.2617	6.2090
	8terms		6.3577	6.3516	6.3334	6.3033	6.2617	6.2090
	10 terms		6.3577	6.3516	6.3334	6.3033	6.2617	6.2090
	12 terms		6.3577	6.3516	6.3334	6.3033	6.2617	6.2090
Timoshenko [30]			6.3876	6.3818	6.3623	6.3330	6.2900	6.2373
RBT [17]			6.3896	6.3832	6.3646	6.3338	6.2912	6.2374
PRESENT	2 terms	1	6.4069	6.4013	6.3844	6.3565	6.3177	6.2683
	4 terms		6.3907	6.3846	6.3663	6.3361	6.2943	6.2413
	6 terms		6.3906	6.3844	6.3662	6.3360	6.2941	6.2412
	8terms		6.3906	6.3844	6.3662	6.3360	6.2941	6.2412
	10 terms		6.3906	6.3844	6.3662	6.3360	6.2941	6.2412
	12 terms		6.3906	6.3844	6.3662	6.3360	6.2941	6.2412

Table 6. Influence of gradient indexes and aspect ratio on dimensionless natural frequencies of CF bi-directional FGB, L/h=5.

Beam Theory		Px	L/h=5 Pz 0	0.2	0.4	0.6	0.8	1
Timoshenko [30]			0.9844	0.9832	0.9796	0.9735	0.9661	0.9576
RBT [17]			0.9848	0.9839	0.9810	0.9764	0.9700	0.9618
PRESENT	2	0	0.9894	0.9885	0.9857	0.9812	0.9749	0.9669
	4		0.9850	0.9840	0.9813	0.9768	0.9705	0.9626
	6		0.9850	0.9840	0.9813	0.9768	0.9705	0.9626
	8terms		0.9850	0.9840	0.9813	0.9768	0.9705	0.9626
	10		0.9850	0.9840	0.9813	0.9768	0.9705	0.9626
	12		0.9850	0.9840	0.9813	0.9768	0.9705	0.9626
Timoshenko [30]			0.8709	0.8697	0.8673	0.8624	0.8564	0.8486
RBT [17]			0.8720	0.8712	0.8687	0.8645	0.8588	0.8516
PRESENT	2	0.4	0.8797	0.8789	0.8765	0.8724	0.8668	0.8597
	4		0.8706	0.8698	0.8673	0.8633	0.8508	0.8492
	6		0.8706	0.8698	0.8673	0.8633	0.8508	0.8492
	8terms		0.8706	0.8698	0.8673	0.8633	0.8508	0.8492
	10		0.8706	0.8698	0.8673	0.8633	0.8508	0.8492
	12		0.8706	0.8698	0.8673	0.8633	0.8508	0.8492
Timoshenko [30]			0.7216	0.7216	0.7177	0.7138	0.7099	0.7021
RBT [17]			0.7225	0.7218	0.7197	0.7163	0.7115	0.7055
PRESENT	2	1	0.7414	0.7407	0.7386	0.7352	0.7304	0.7244
	4		0.7225	0.7218	0.7198	0.7164	0.7118	0.7059
	6		0.7225	0.7218	0.7198	0.7164	0.7118	0.7059
	8terms		0.7225	0.7218	0.7198	0.7164	0.7118	0.7059
	10		0.7225	0.7218	0.7198	0.7164	0.7118	0.7059
	12		0.7225	0.7218	0.7198	0.7164	0.7118	0.7059

Table 7. Influence of gradient indexes and aspect ratio on dimensionless natural frequencies of CF bi-directional FGB, L/h=20.

Beam Theory		Px	L/h=20 Pz 0	0.2	0.4	0.6	0.8	1
Timoshenko [30]			1.0126	1.0126	1.0087	1.0029	0.9970	0.9873
RBT [17]			1.0130	1.0120	1.0090	1.0040	0.9971	0.9884
PRESENT	2 terms	0	1.0178	1.0168	1.0138	1.0088	1.0019	0.9932
	4 terms		1.0130	1.0120	1.0090	1.0040	0.9972	0.9885
	6 terms		1.0130	1.0120	1.0090	1.0040	0.9972	0.9885
	8terms		1.0130	1.0120	1.0090	1.0040	0.9972	0.9885
	10 terms		1.0130	1.0120	1.0090	1.0040	0.9972	0.9885
	12 terms		1.0130	1.0120	1.0090	1.0040	0.9972	0.9885
Timoshenko [30]			0.8955	0.8935	0.8916	0.8876	0.8798	0.8721
RBT [17]			0.8950	0.8941	0.8914	0.8870	0.8810	0.8733
PRESENT	2 terms	0.4	0.9046	0.9037	0.9010	0.8966	0.8905	0.8827
	4 terms		0.8949	0.8940	0.8914	0.8870	0.8809	0.8732
	6 terms		0.8949	0.8940	0.8914	0.8870	0.8809	0.8732
	8terms		0.8949	0.8940	0.8914	0.8870	0.8809	0.8732
	10 terms		0.8949	0.8940	0.8914	0.8870	0.8809	0.8732
	12 terms		0.8949	0.8940	0.8914	0.8870	0.8809	0.8732
Timoshenko [30]			0.7392	0.7392	0.7373	0.7333	0.7275	0.7216
RBT [17]			0.7394	0.7386	0.7364	0.7328	0.7278	0.7214
PRESENT	2 terms	1	0.7589	0.7582	0.7559	0.7522	0.7470	0.7405
	4 terms		0.7392	0.7385	0.7363	0.7326	0.7276	0.7213
	6 terms		0.7392	0.7385	0.7363	0.7326	0.7276	0.7213
	8terms		0.7392	0.7385	0.7363	0.7326	0.7276	0.7213
	10 terms		0.7392	0.7385	0.7363	0.7326	0.7276	0.7213
	12 terms		0.7392	0.7385	0.7363	0.7326	0.7276	0.7213

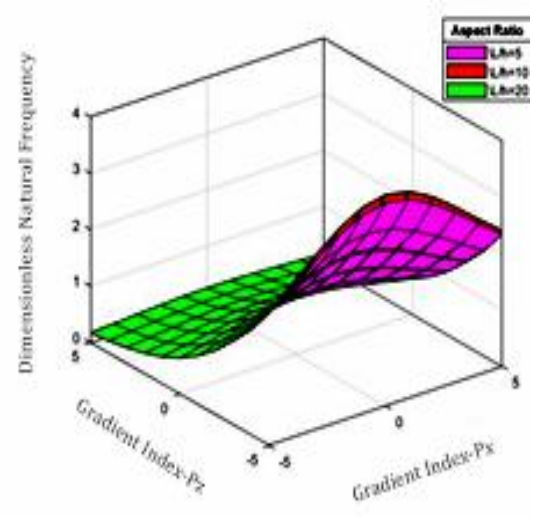

Fig. 6. Changes in dimensionless natural frequencies of CF beam at various aspect ratios along the x-direction gradient

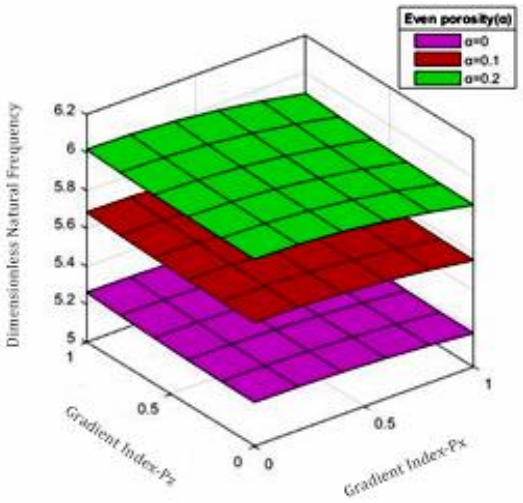

Fig. 9. Dimensionless natural frequencies of CC beam with even porosity at aspect ratio L/h=5

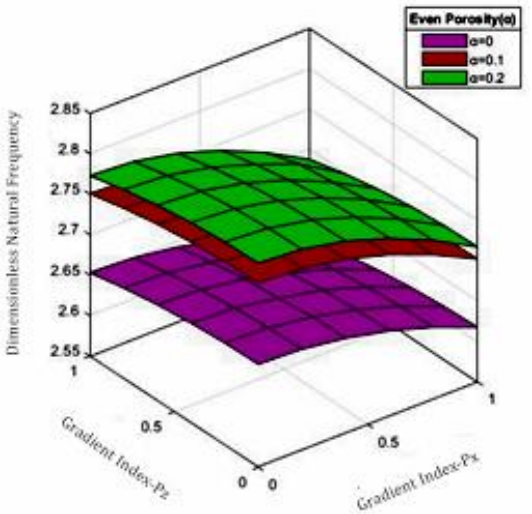

Fig. 7. Dimensionless natural frequencies of SS beam with even porosity at aspect ratio L/h=5

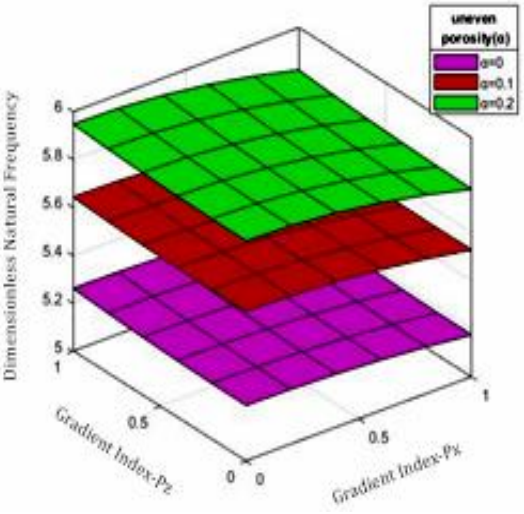

Fig. 10. Dimensionless natural frequencies of CC beam with uneven porosity at aspect ratio L/h=5

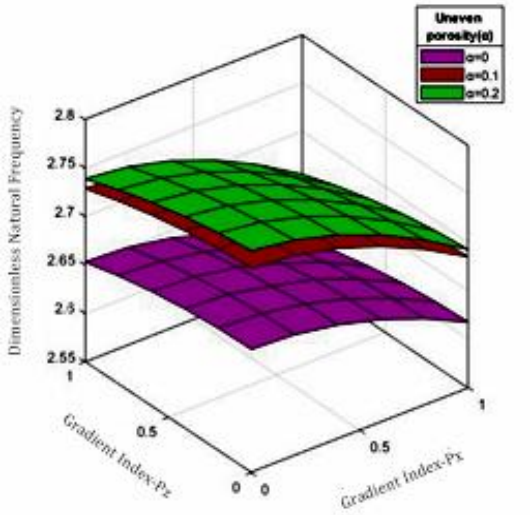

Fig. 8. Dimensionless natural frequencies of SS beam with uneven porosity at aspect ratio L/h=5

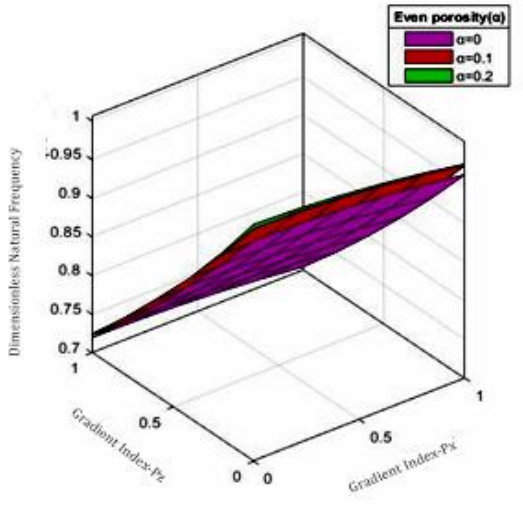

Fig. 11. Dimensionless natural frequencies of CF beam with even porosity at aspect ratio L/h=5

Table 8. Influence of gradient indexes and porosity distribution on dimensionless natural frequencies of SS bi-directional FGB at aspect ratio L/h=5

Px & Pz	Even Porosity				Uneven Porosity			
	0	0.1	0.2	0.3	0	0.1	0.2	0.3
0	2.6774	2.7781	2.8193	2.8528	2.6774	2.7612	2.7843	2.7985
0.2	2.6738	2.7708	2.8082	2.8376	2.6738	2.7573	2.7805	2.7944
0.4	2.6615	2.7559	2.7897	2.8154	2.6615	2.7453	2.7649	2.7771
0.6	2.6447	2.7333	2.7628	2.7861	2.6447	2.7228	2.7420	2.7524
0.8	2.6192	2.7032	2.7305	2.7499	2.6192	2.6937	2.7110	2.7196
1	2.5792	2.6656	2.6901	2.7068	2.5792	2.6570	2.6723	2.6793

Table 9. Influence of gradient indexes and porosity distribution on dimensionless natural frequencies of CC bi-directional FGB at aspect ratio L/h=5

Px & Pz	Even Porosity				Uneven Porosity			
	0	0.1	0.2	0.3	0	0.1	0.2	0.3
0	5.2328	5.6552	5.9867	6.3282	5.2328	5.6249	5.9175	6.2110
0.2	5.2310	5.5870	5.9698	6.3005	5.2310	5.5623	5.9127	6.2040
0.4	5.2255	5.5745	5.9479	6.2675	5.2255	5.5537	5.8995	6.1854
0.6	5.2163	5.5578	5.9212	6.2293	5.2163	5.5398	5.8791	6.1577
0.8	5.2032	5.5368	5.8896	6.1860	5.2032	5.5209	5.8523	6.1224
1	5.1862	5.5114	5.8532	6.1376	5.1862	5.4971	5.8197	6.0804

Table 10. Influence of gradient indexes and porosity distribution on dimensionless natural frequencies of CF bi-directional FGB at aspect ratio L/h=5

Px & Pz	Even Porosity				Uneven Porosity			
	0	0.1	0.2	0.3	0	0.1	0.2	0.3
0	0.9850	1.0006	1.0142	1.0256	0.9850	0.9944	1.0014	1.0057
0.2	0.9255	0.9381	0.9488	0.9571	0.9255	0.9317	0.9355	0.9364
0.4	0.8673	0.8777	0.8861	0.8922	0.8673	0.8714	0.8731	0.8720
0.6	0.8108	0.8193	0.8260	0.8305	0.8108	0.8134	0.8137	0.8114
0.8	0.7560	0.7631	0.7685	0.7718	0.7560	0.7576	0.7571	0.7542
1	0.7059	0.7092	0.7135	0.7160	0.7059	0.7042	0.7032	0.7000

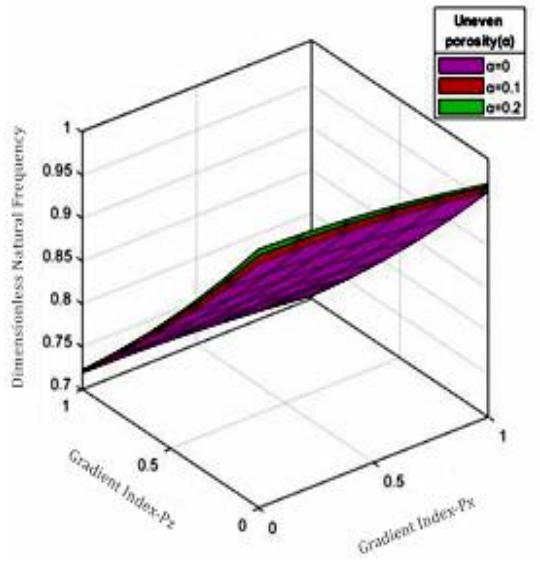

Fig. 12. Dimensionless natural frequencies of CF beam with uneven porosity at aspect ratio L/h=5

Figure 7 and Figure 8 show the dimensionless free vibration versus the gradient indexes in length (p_x) and thickness (P_z) direction for different porosity distribution patterns when α = 0.1. It can be observed that the difference between different porosity distribution patterns can be increased with an increase in the porosity index (α). "Which indicates that the porosity distribution in thickness (z) direction has a greater influence on vibration than axial porosity (x direction) distribution." On the other hand, free vibration is more in even porosity distribution than in uneven porosity distribution.

Figure 9, Figure 10, Figure 11, and Figure 12 illustrate the dimensionless free versus gradient indexes in length (P_x) and thickness (P_z) direction of the beam and the total volume fraction of porosity in different modes, respectively. It can be seen that the sensitivity of free vibration to the gradient index of the beam and total volume

fraction of porosity has improved with an increase in the vibration mode number.

Table 8 shows the free vibration value of the SS beam which increases with an increase in porosity index, and decreases with an increase in gradation exponents in the x and z directions. Vibration value is more in even porosity distribution as compared with uneven porosity distribution.

Table 9 shows the free vibration value of the CC beam which increases with an increase in porosity index, and decreases with an increase in gradation exponents in the x and z directions. Vibration value is more in even porosity distribution as compared with uneven porosity distribution.

Table 10 shows the free vibration value of the CF beam which increases with an increase in porosity index, and decreases with an increase in gradation exponents in the x and z directions. Vibration value is more in even porosity distribution as compared with uneven porosity distribution.

It can be noted that free vibration increases with the porosity coefficient and this impact is more significant at a high porosity value, which is caused by a reduction in flexible rigidity of the FG beam at a high porosity value. In addition, it can be observed that the vibration decreases with an increase in gradient index, this is for even and uneven types of porosity. When the gradient index is zero (p=0) the beam is pure metal with less stiffness. As the gradient index (p) tends to infinity, a beam is a pure ceramic with high stiffness which means less vibration.

4. Conclusions

Two directional FG porous beams were analyzed for the behavior of free vibration, subjected to various boundary conditions (SS, CC, and CF).

Considering these boundary conditions with different aspect ratios and gradation exponents in x and z directions. n^{th}-order shear deformation theory was adapted to determine free vibration with even and uneven porosity distribution. Based on power-law distribution, the effective properties of FG porous beams in two directions were determined.

The effect of boundary conditions, distribution of porosity, aspect ratios, and gradation exponents on free vibration analysis through several numerical illustrations was highlighted.

The computed results are compared to those with earlier investigations in terms of dimensionless free vibration. The calculated outcomes are found to have a very good correlation with earlier ones. Aspect ratios, gradient indexes, and boundary conditions' impact on 2D-FGBs' free vibration were explored.

The most significant findings w.r.t nonporous FGBs are listed below:

- The gradient indexes have a significant impact on the dimensionless free vibration of 2D-FGBs. However, the gradient index's impact in the x-direction is more profound than its impact in the z-direction.
- The shear deformation effect on the vibration of 2D-FGBs increases as the aspect ratio increases. CC 2D-FGB is found to be significantly more susceptible to the shear deformation effect than the other 2D-FGB models.
- CC beams experience the highest first free vibration, followed by SS and CF beams.
- By choosing appropriate gradient indexes, vibration behaviors of 2D-FGBs may be regulated to match the design requirements.
- The shear deformation impact is quite significant, especially for thick beams, and the proposed theory yields accurate findings and is effective in resolving vibration behaviors of 2D-FGBs.
- The suggested two-directionally porous beam model is used to examine the free vibration behavior of two-directional porous beams.
- The most significant findings w.r.t porous FGBs are listed below:
- As the volume percentage of porosity increases close to the middle surface, free vibration will increase for the same total volume fraction of porosity.
- The effect of porosity distribution in a thickness direction is more dominant than the effect of axial direction on free vibration.
- The porosity parameter is a crucial parameter that must be considered in the design of modern structures and the percentage of porosity in structure can be affected considerably in its performance and response". The proposed method shall also be useful to analyze the shear deformation of FGBs, where these FGB surfaces are subjected to high temperatures at one end and low temperatures at the other end.

Nomenclature

x,y, z	Different coordinates along length, width, and thickness directions of beam
2D	Two dimensional
FGB	Functionally graded beam
SS	Simply supported
CC	Clamped-clamped
CF	Clamped free
FGM	Functionally graded material
L	Length[m]
h	Height[m]
$\frac{\partial w_0}{\partial x}$	Bending slope
ϕ	Shear slope.
V_f	Volume fraction
P_z	Gradient index in the thickness direction
p_x	Gradient index in the length direction
CBT	Classical beam theory
K	Shear correction factor
f(z)	Shear shape function
FG	Functionally graded
3D	Three dimensional
FGP	Functionally graded plate
HSD	Higher order deformation
E	Modulus of elasticity[GPa]
μ	Poisson's ratio
ρ	Mass density[Kg/m3]
α	Coefficient of porosity
[Ski]	Stiffness matrix
[Mki]	Mass matrix
δU	Strain energy
δk	Kinetic energy

References

[1] Li, C., Shijie, Z. and Chen, D., 2020. Size-dependent isogeometric analysis of bi-directional FG micro beams reinforced by graphene nanoplatelets. *Mechanics Based Design of Structures and Machines*, pp. 1-19.

[2] Asemi, S.R., Ali, F.O., Hamid, R.A.Z. and Mohammadi, M., 2014. Influence of initial stress on the vibration of double-piezoelectric-nanoplate systems with various boundary conditions using DQM. *Physica E: Low-dimensional Systems and Nanostructures, 63*, pp. 169-179.

[3] Aydogdu, M. and Taskin, v., 2007. Free vibration analysis of FGBs with simply supported edges. *Materials & Design, 28*(5), pp. 1651-1656.

[4] Al-Zahrani and Meshal, A., 2022. Free Vibration Analysis of 2D FG Strip Beam using Finite Element Method. Journal of Applied and Computational Mechanics.

[5] Barati, A., Hadi, A., Nezad, M.Z. and Noroozi, R., 2022. On vibration of bi-directional FG nanobeams under magnetic field. *Mechanics Based Design of Structures and Machines, 50*(2), pp. 468-485.

[6] Bellifa, H., Halim, K.B., Hadji, L., Sid Ahmed, M.H. and Tounsi, A., 2016. Bending and free vibration analysis of FGPs using a simple shear deformation theory and the concept of the neutral surface position. *Journal of the Brazilian Society of Mechanical Sciences and Engineering, 38*(1), pp. 265-275.

[7] Daneshmehr, A., Amir, R. and Hadi, A., 2015. Size-dependent free vibration analysis of nanoplates made of FGM based on nonlocal elasticity theory with high order theories. *International Journal of Engineering Science, 95*, pp. 23-35.

[8] Ebrahimi, F. and Barati, M.R., 2016. A nonlocal higher-order shear deformation beam theory for vibration analysis of size-dependent FG nanobeams. *Arabian Journal for Science and Engineering, 41*(5), pp. 1679-1690.

[9] Hadji, L. and Bernard, F., 2020. Bending and free vibration analysis of FGBs on elastic foundations with analytical validation. *Advances in materials Research, 9*(1), pp. 63-98.

[10] Zaoui, F.Z., Hanifi, H., Lemya, A., Abderahman, O., Meradjah, M., Tounsi Abdelouahed and Ouinas Djamel., 2017. Free vibration analysis of FGBs using a higher-order shear deformation theory. *Mathematical Modelling Of Engineering Problems, 4*(1), pp. 7-12.

[11] Gorgani, H.H., Adeli, M.M. and Hosseini, M., 2019. Pull-in behavior of FG micro/nano-beams for MEMS and NEMS switches. *Microsystem Technologies, 25*(8), pp. 3165-3173.

[12] Hebbar, N., Hebber, I., Ouinas, D. and Bourada, M., 2020. Numerical modeling of bending, buckling, and vibration of FGBs by using a higher-order shear deformation theory. *FratturaedIntegritàStrutturale, 14*(52), pp. 230-246.

[13] Huang, Y., Yang, L.E. and Luo, Q.Z., 2019. Free vibration of axially FG Timoshenko beams

with non-uniform cross-section. *Composites Part B: Engineering, 45*(1), pp. 1493-1498.
[14] Jha, D.K., Tarun, K. and Ram Kumar Singh, 2013. Higher order shear and normal deformation theory for natural frequency of FG rectangular plates. *Nuclear Engineering and Design, 250*, pp. 8-13.
[15] Armagan k., 2018. Free vibration analysis of two directional FGBs using third-order shear deformation theory. *Composite Structure, 189* (10), pp. 127-136.
[16] Ketabdari, M.J., Allahverdi, A., Boreyri, S. and Ardestani, M.F., 2016. Free vibration analysis of homogeneous and FGM skew plates resting on variable Winkler-Pasternak elastic foundation; *Mechanics & Industry, 17*(1).
[17] Larbi, L.O., Houari, M.S.A. and Tounsi, A., 2013. An efficient shear deformation beam theory based on neutral surface position for bending and free vibration of FGBs. *Mechanics Based Design of Structures and Machines, 41*(4), pp. 421-433.
[18] Mohammadi, M., Farajpour, A., Goodarzi, M. and Shehni nezhad pour, H., 2014. Numerical study of the effect of shear in-plane load on the vibration analysis of graphene sheet embedded in an elastic medium. *Computational Materials Science, 82*, pp. 510-520.
[19] Ohab-Yazdi, Sayed Mohammad Kazem, and Mehran Kadkhodayan, 2021. Application of Bi-Directional FGM model for free vibration analysis of rotating Euler-Bernoulli Nanobeams. *Mechanics of Advanced Composite Structures, 8*(2), pp. 389-399.
[20] Nguyen, T.K., Vo, T.P. and Thai, H.T., 2013. Static and free vibration of axially loaded FGBs based on the first-order shear deformation theory. *Composites Part B: Engineering, 55*, pp. 147-157.
[21] Rahmani, O. and Pedram, O., 2014. Analysis and modeling of the size effect on vibration of FG nanobeams based on nonlocal Timoshenko beam theory. *International Journal of Engineering Science, 77*, pp. 55-70.
[22] Safarabadi, M., Mohammadi, M., Farajpour, A. and Goodarzi, M., 2015. Effect of surface energy on the vibration analysis of rotating nanobeam. *Journal of Solid Mechanics, 7*(3), pp. 299-311.
[23] Şimşek, M., 2010. Fundamental frequency analysis of FGBs by using different higher-order beam theories. *Nuclear Engineering and Design, 240*(4), pp. 697-705.
[24] Babaei, Masoud, Kamran Asemi, and Faraz Kiarasi, 2020. Static response and free-vibration analysis of an FG annular elliptical sector plate made of saturated porous material based on 3D finite element method. *Mechanics Based Design of Structures and Machines*, 1-25.
[25] Talha, M., and Singh, B., 2010. Static response and free vibration analysis of FGM plates using higher order shear deformation theory, *Applied Mathematical Modelling, 34*(12), pp. 3991-4011.
[26] Thai, H.T. and Vo, T.P., 2012. Bending and free vibration of FGBs using various higher-order shear deformation beam theories. *International journal of mechanical sciences, 62*(1), pp. 57-66.
[27] Vo, T.P., Thai, H.T., Nguyen, T.K. and Inan, F., 2014. Static and vibration analysis of FGBs using refined shear deformation theory. *Meccanica, 49*(1), pp. 155-168.
[28] Simsek, M., 2015. Bi-Directional FGM for free and forced vibration of Timoshenko beams with various boundary conditions. *Compos Struct. 133*(1).
[29] Sayyad, A.S. and Ghugal, Y.M., 2017. A unified shear deformation theory for the bending of isotropic, FG, laminated, and sandwich beams and plates. *Int. j appl. Mechanics, 9*(1).
[30] Razouki, A., Boutahar, L. and Bikri, K.E., 2020. The Free Vibration Analysis of Thick FGBs Accounting Higher Order Shear Deformation Theory With Differential Transform Method. *Int. J Adv. Res Sci. Eng. Technol, 11*(7), pp. 1-10.
[31] Slimane, M., Samir, B., Hakima, B. and Hadj Mostefa, A., 2019. Free vibration analysis of FGPs with porosities. *International Journal of Engineering Research & Technology (IJERT), 8*(03), pp. 143-147.
[32] Mehdianfar, Pejman, Yasin Shabani, and Korosh Korshidi, 2022. Natural frequency of Sandwich Beam Structures with 2D-FG Porous Layers Based on Novel Formulations. *International Journal of Engineering, 35*(11).
[33] Asemi, Kamran, Masoud Babaei, and Faraz Kiarasi, 2020. Static, natural frequency, and dynamic analyses of FG porous annular sector plates reinforced by graphene platelets. *Mechanics Based Design of Structures and Machines*, pp. 1-29.
[34] Babaei, M., Asemi, k., and Safarpour, p., 2019. Natural frequency and dynamic analyses of FG saturated porous beam resting on a viscoelastic foundation based on higher order beam theory. *Journal of Solid Mechanics, 11*(3), pp. 615-634.
[35] Mohammadi, M. and Rastgoo, A., 2019. Nonlinear vibration analysis of the viscoelastic composite nanoplate with three directionally imperfect porous FG cores. *Structural Engineering and Mechanics an Int'l Journal, 69*(2), pp. 131-143.
[36] Kim, J., Kamal, K. and Reddy, J.N., 2019. Bending, free vibration, and buckling of

modified couples stress-based FG porous micro-plates. *Composite Structures, 209*, pp. 879-888.

[37] Chen, D., Shijie, Z., Wang, Y., Yang, L. and Li, Z., 2020. Nonlinear free vibration analysis of a rotating two-dimensional FG porous micro-beam using isogeometric analysis. *European Journal of Mechanics - A/Solids, 84*.

[38] Li, S., Shijie, Z. and Chen, D., 2020. Porosity-dependent isogeometric analysis of bi-directional FGPs. Thin-Walled Structures, 156.

[39] Bathini, S.R., Vijay Kumar Reddy, K., and Ankanna, C., 2020. Free vibration behavior of bi-directional FGPs with porosities using a refined first-order shear deformation theory. *Journal of Computational Applied Mechanics, 51*(2), pp. 374-388.

[40] Kumar, Y., 2022. Effect of Elastically Restrained Edges on Free Transverse Vibration of FG Porous Rectangular Plate. *Mechanics of Advanced Composite Structures, 9*, pp. 335 – 348.

[41] Vasaraa, D., Kharea, S., Malgurib, A. and Kumar, R., 2022. Numerical Investigation on Free Vibration Response of Bi-Directional Porous FG Circular/Annular Plates. *Mechanics of Advanced Composite Structures, 9*, pp. 243 – 262.

[42] Karamanlı, A., 2018. Analytical solutions for buckling behavior of two directional FGBs using a third-order shear deformable beam theory. *Academic Platform Journal of Engineering and Science, 6*(2), pp. 164-178,

[43] Souhir Zghal, 2020. Static bending analysis of beams made of FG porous materials, *Mechanics Based Design of Structures and Machines, 50*(3), pp. 1012-1029.